

Tunable Dewatering Behavior of Montmorillonite Suspension by Adjusting Solution pH and Electrolyte Concentration

Yingdi Dong ¹, Hongliang Li ¹, Yuping Fan ¹, Xiaomin Ma ¹, Dong Sun ¹, Yanhong Wang ^{2,3}, Zhiyong Gao ^{2,3,*} and Xianshu Dong ^{1,*}

¹ College of Mining Engineering, Taiyuan University of Technology, Taiyuan 030024, China; dongydyd@163.com (Y.D.); lihongliang222@126.com (H.L.); 19880628fyp@163.com (Y.F.); near0369@163.com (X.M.); Sundong@tyut.edu.cn (D.S.)

² School of Minerals Processing and Bioengineering, Central South University, Changsha 410083, China; yanhong.wang@csu.edu.cn

³ Key Laboratory of Hunan Province for Clean and Efficient Utilization of Strategic Calcium-Containing Mineral Resources, Central South University, Changsha 410083, China

* Correspondence: zhiyong.gao@csu.edu.cn (Z.G.); dongxianshu@tyut.edu.cn (X.D.)

Received: 2 February 2020; Accepted: 23 March 2020; Published: 25 March 2020

Abstract: Montmorillonite is always a troublemaker for the dewatering in coal processing since its existence can decrease the rates of sedimentation and filtration of coal slurry. To eliminate the adverse effect of montmorillonite, adjusting the slurry pH and adding electrolytes are always the key methods. However, the underlying mechanism still needs to be further studied. The dewatering of Na-montmorillonite (Na-Mt) suspensions has been studied as a function of NaCl concentration (10^{-3} , 10^{-2} , and 10^{-1} M) at different pH values (6.0, 7.7, 8.1, 9.2). The point of zero charge of edge surface of Na-Mt ($pH_{PZC,edge}$) appeared at the pH value of 6.8. The sedimentation and rheology experiments described the coagulation and flow behaviors of Na-Mt suspensions, respectively. The Na-Mt suspension coagulated spontaneously at low salt concentration with the pH \sim 6.0. For the pH $>$ $pH_{PZC,edge}$, the height of the sediment bed reduced and apparent viscosity increased with the increase of the electrolyte concentration. The filtration properties were evaluated on the basis of Darcy's law. The obtained result clearly demonstrated that the filtration rate was accelerated with the increase of pH and electrolyte concentration. The modes of particle association and its effect on filtration performance were discussed. Moreover, a comparison with related results from the literature was performed. At pH \sim 6 and low electrolyte concentration, the positively charged Edge surfaces and negatively charged Face surfaces coagulate rapidly to form a sealed structure by electrostatic attraction. Furthermore, inside this sealed structure, the water molecules cannot be removed in the filtration process easily. However, by increasing the electrolyte concentration at pH $>$ $pH_{PZC,edge}$, the gradually formed Face/Face structure increases the filtration rate sharply because of the inhibiting effect of the electric double layer (EDL) and the osmotic expansion. Therefore, adjusting solution conditions of the aqueous suspension to tune the particle coagulation behavior is one of the effective methods to solve the problem of montmorillonite dewatering.

Keywords: montmorillonite; zeta potential; rheology; filtration; particle association mode

1. Introduction

With the scarcity of high-grade mineral resources, the separation process of lower-grade clay-bearing ore brings about more challenges in mineral processing plants. As has been proposed, montmorillonite characteristics have great influence on the slurry rheology, surface properties of

tailing, and efficiency of reagents. Therefore, raw ore containing montmorillonite leads to adverse effects on the process performance, such as floatation, dewatering, and wastewater treatment. Thus, understanding of surface properties, rheological characteristics, and particle interaction of montmorillonite are essential when dealing with the aforementioned difficulties in the dewatering process [1].

Yield stress and viscosity are the essential factors to evaluate rheological properties of aqueous suspensions of montmorillonite. The increased solid concentration of montmorillonite suspension leads to an increase in yield stress and apparent viscosity. It also affects the rheological behaviors, which are transformed from Newtonian to Bingham plastic to shear thinning material with yield stress. In particular, the initial stress increases with aging time because of the full hydration in enough time [2,3]. It was shown that the addition of ionic strength (0.02–0.2 M) decreased the apparent viscosity and changed rheological behaviors of the suspension. In addition, the divalent cation salts were more effective in reducing the yield stress and apparent viscosity than monovalent cation salts [3]. The systems with the reagent of polyacrylamide (PAM) and montmorillonite were always discovered in the process of dewatering. The molecular simulation method established that the viscosity of the PAM between hydrated clay layers reduced with an increase of either temperature (from 298 to 343 K) or shear rate (from 2.27×10^9 to $1.36 \times 10^{10} \text{ s}^{-1}$) [4]. In the research of montmorillonite with adsorbed phosphate additives, the magnitude of yield stress was remarkably smaller than with pure montmorillonite samples. As a result, the adsorbed phosphate additives formed a steric layer and decreased the strength of the attractive interparticle forces. Especially at alkali pH, the yield stress was entirely dispersed with the presence of adsorbed phosphate [5]. The montmorillonite coagulated rapidly in the suspension of high NaCl concentration, and the floc size distribution was approximate to log normal [6]. The scaling relation between the maximum size of floc (D_{\max}) and the shear rate (G) was an approach to $D_{\max} \sim G^{-\gamma}$, for which a value of γ close to 0.5 revealed an equilibrium between the formation and breakup of flocs. However, when the value of γ was more than 0.5, the flocs were restructured directly [7].

There are several fundamental parameters that could determine the interaction of particles, such as layer charge, cation exchange, edge charge density, and particle structure. At a low pH value, the card-house structure is formed due to Edge⁺–Face[−] interaction. However, at a high pH value, Face[−]–Face[−] interaction causes the band-like structure [8]. By using extended DLVO theory, the total Face–Face, Edge–Edge, and Face–Edge energy of interaction in Na-Mt suspension on the basis of DLVO theory, the yield stress of the suspension and viscosity of the flocs are decreased from acid to alkali, which is mainly caused by the interaction of face-to-edge attraction [9]. A quite different rheological behavior was discovered from a composite of Na-montmorillonite and needle-shaped sepiolite. The suspension of these two ingredients showed a very low or no yield stress at acid pH and approached the maximum value of pH 8–12. Because the magnesium is released from sepiolite at low pH, its hydrolysis products are formed and adsorbed on particle surfaces gradually with the increase of the pH value [10]. The acid–base environment shows a significant influence on the rheological properties of montmorillonite suspension. Nevertheless, it has little effect on the zeta potential. Montmorillonite particles in water did not display a point of net zero charge (PZC) or the isoelectric point. The results of zeta potential are negatively charged at all pH [11,12]. The point of zero charge of zero proton charge (PZNPC) for $\sigma_{0,H} = 0$ is appropriate for surface charge heterogeneity of montmorillonite lamellae. Therefore, the $\text{pH}_{\text{PZC,edge}}$ of the amphoteric edge sites ($\text{pH}_{\text{PZC,edge}}$) is distinct [13–15]. For the Wyoming montmorillonite, $\text{pH}_{\text{PZC,edge}}$ is in the pH range from 6 to 7 with the variation of ionic strength in the suspension [16]. The diverse acids (such as fulvic and polyacrylic acids), the electrolyte type, and its concentration (such as 10^{-3} – 10^{-1} M KNO_3 , 10^{-3} – 10^{-2} M NaCl) were used to analyze the $\text{pH}_{\text{PZC,edge}}$ with the pH value of 6.5 [9,15,17].

In the absence of Ca^{2+} ion montmorillonite suspensions, the high basal surface repulsion leads to clay platelets, which forms in an Edge–Edge orientation. However, with the addition of Ca^{2+} ions, the structure of clay platelets is converted from both Edge–Edge and Edge–Face to a Face–Face orientation [18]. The high permeability of water and ions was observed in Ca-montmorillonite because of the extra-lamellar swelling between tactoids, instead of between the single platelets [19,20]. Surface charge density is an important factor in affecting ion–ion correlation in montmorillonite suspension.

In a composed system with counterions (Na^+ and Ca^{2+}), Ca^{2+} leads montmorillonite to a nonswelling behavior in a higher surface charge density. Otherwise, a swelling behavior is observed when Na^+ dominates in the slit [20]. The combination of wide-angle X-ray scattering (WAXS), small-angle X-ray scattering (SAXS), and transmission X-ray microscopy (TXM) provided an efficient method to understand the coagulation mechanism of Na-montmorillonite. At a neutral pH, the Na-Mt is completely coagulated by the interactions of Face^- – Face^- , and the stacks of these particles have a slight mismatch between layers [21,22]. There are two main driving forces that determine the clay minerals' surface chemistry: ion pairing and hydration energy of ions. The weakly paired ions (I^- and Cs^+) with the minimum hydration energy interact strongly with the clay minerals' surface. On the contrary, the high hydration energy ions (Na^+ and F^-) have a high charge density to restrain their interaction with the clay minerals' surface [23].

Besides, the effect of pH value and ionic strength on the coagulation structure of montmorillonite suspension reflects on the sedimentation and filtration behavior. The influence of pH value on the sedimentation rate is remarkable at low salt concentration for the dominant appearance of the Edge/Face association [24]. However, the limited effect of pH value on sediment height at higher salt concentration was regarded as the shielding effect by the compression of the electric double layer [25]. Particle association has an important effect on the filtration behavior such as thickness, moisture ratio, and permeability [26]. An addition of clay hybrids decreases low-temperature low-pressure and high-temperature high-pressure fluid loss, which is greatly related to the restructure of clay platelet association [27]. The filtration behavior is enhanced with an addition of the water-soluble ionic liquid and the filtration control additive (PASV), on account of the cation exchange and the elimination of the stabilization of the bentonite dispersion state, respectively [28,29].

In particular, researchers show much concern for the pH-dependent charges on broken edges of montmorillonite layers and the different coagulation modes between particles. In this paper, the height of the sediment bed, rheological behavior, and filtration performance of Na-Mt suspensions are investigated by analyzing particle surface charge properties, interactions between particles, and association modes as a function of the electrolyte concentrations and pH.

2. Materials and Methods

2.1. Material Preparation and Characterization

The Na-montmorillonite raw sample purchased from Chifeng Liaoyu Coal Company was composed mainly of Na-Mt with low amounts of quartz and cristobalite. The montmorillonite–water suspension was prepared by adding the samples and water in a desired solid concentration. Analytical grade HCl, NaOH, and NaCl were used as Na-Mt modified reagent for acid–base environment regulation and cation exchange in the present study. The size of analytical grade Al_2O_3 and SiO_2 powders were 1 μm and 50 nm, respectively. All the water used in this work was ultrapure water distilled and deionized by UPR-II series ultrapure water machine (ULUPure, Chengdu, China) with the electrical resistivity of 18.2 $\text{M}\Omega/\text{cm}$, heavy metal ions ≤ 0.1 ppb, and microparticles ≤ 1 /mL; by doing so, the effects of impurities on the suspension and aggregation behaviors were minimized.

The purification method [30] consisted of replacing the exchangeable cations with Na^+ ions followed by washing with water. Washing removed excess salts and also enabled fine impurities to be separated. The raw Na-montmorillonite sample (30 g) was carefully dispersed in 1 L of 1 M NaCl solution by stirring at 500 rpm for about 12 h and then shaking overnight. Afterwards, the suspension was separated into four centrifuge bottles and then centrifuged at 3000 rpm for 5 min. This cycle of Na^+ exchange procedure was repeated three times. The sediment of the Na^+ -exchanged clay mineral was washed with water. The washing procedure was the same as that for the Na^+ exchange with stir, shake, and centrifugation cycles, which was also repeated three times. Finally, the purified Na-montmorillonite sample had achieved sufficient exchange and removed excess salts and fine impurities. The cation exchange capacity (CEC) of the purified Na-Montmorillonite was 103.8 cmol/kg .

The raw Na-Mt sample (2 g), Na⁺-exchanged sample without washing (200 mL), and purified sample (200 mL) were all dried in an oven at 105 °C for the X-ray diffraction (XRD) measurements. Figure 1 displays the XRD pattern of the sample, which was measured by a MiniFlex 600 (Rigaku, Tokyo, Japan) with Cu K α radiation at 40 kV voltage and a scanning speed of 5°/min from 0° to 70°. It shows that the purified Na-Mt materials had nearly no impurities, indicating that the sample was high-purity Na-Mt. Figure 1a shows the mineral composition of the raw sample of Na-Mt, and low amounts of quartz and cristobalite. After replacing the exchangeable cations with Na⁺ ions and centrifugation, the surface of the particles was covered by the residuals of sodium chloride as can be seen in Figure 1b. Then, by applying the washing procedure and centrifugation, the heights of the diffraction peaks of Na-Mt were apparently greater than those of preceding samples at $2\theta = 6.1^\circ$, which are shown in Figure 1c. The increased crystal component of Na-Mt indicated that the sample was extremely purified.

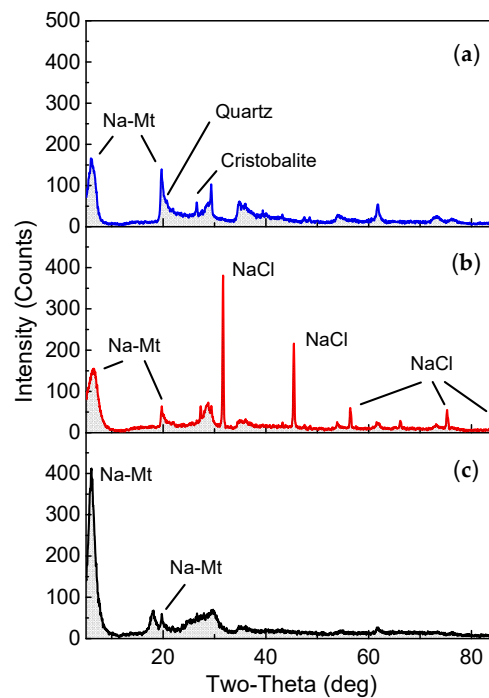


Figure 1. XRD pattern of the purification process of the Na-montmorillonite samples: (a) the raw sample; (b) the sample after Na⁺-exchange and centrifugation procedure; (c) the purified sample after washing with ultrapure water and centrifugation.

The particle size distribution of the montmorillonite–water suspension was measured by a Microtrac S3500 laser diffraction particle size analyzer (MICROTRAC MRB, Osaka, Japan). The suspension was fully dispersed by ultrasound for 10 min to show the particle size distribution. Figure 2 depicts that the median diameter (d_{50}) of montmorillonite particles was around 500 nm.

The morphologies of the raw and highly purified Na-montmorillonite particles are shown in Figure 3, which was taken with a JSM-7100F scanning electron microscope (SEM, JEOL Ltd., Tokyo, Japan). The purified Na-Mt sample was dried in an oven at 105 °C. The SEM image of the raw Na-Mt sample was taken at an accelerating voltage of 15.0 kV and a working distance of 12.1 mm, and the SEM image of the purified Na-Mt sample was taken at an accelerating voltage of 5.0 kV and a working distance of 13.7 mm. As can be observed, most of the surface area of the powder was contributed by the lamellar of the montmorillonite rather than spherical in shape.

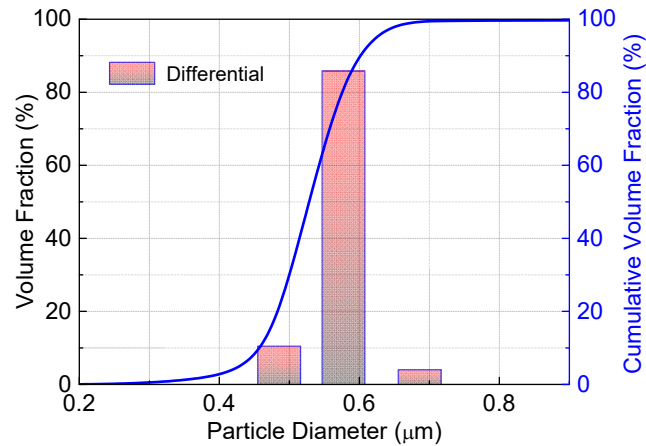


Figure 2. The particle size distribution of the highly purified Na-montmorillonite.

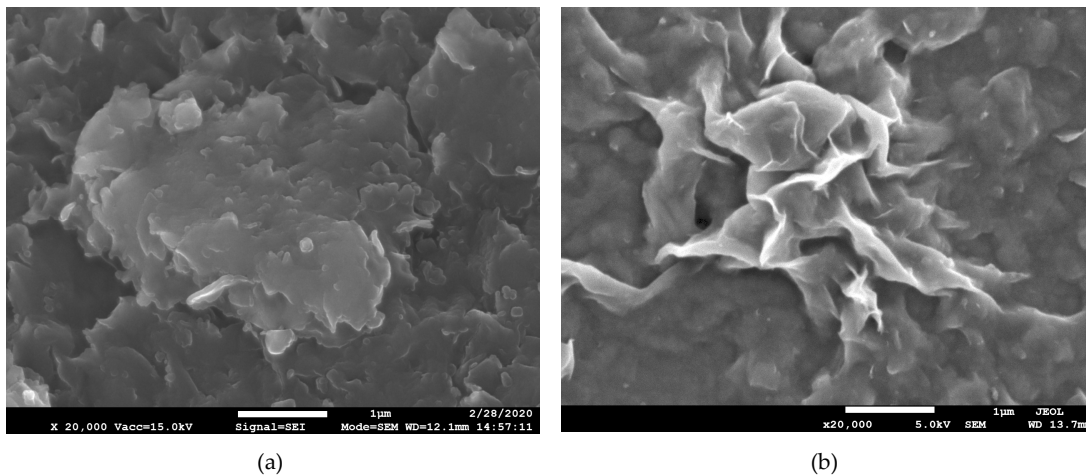


Figure 3. SEM images of Na-montmorillonite powder 20k × magnification: (a) raw sample; (b) highly purified sample.

All suspensions were diluted by mixing the purified Na-montmorillonite with ultrapure water to the required mass ratio of 1:1000. The initial or natural pH of these suspensions was 7.7. All the filtration experiments were performed in a thermostat water bath at the desired temperature of 25 °C. Three different ionic strengths of 10^{-3} , 10^{-2} , and 10^{-1} M of NaCl were used in the experiments. A known volume of the Na-Mt suspension with a known concentration (C_c) of 1 g/L at an appropriate ionic strength was continuously stirred at 500 rpm overnight to mix extensively. When pH adjustment was required, droplets of concentrated HCl and NaOH were added. Concentrated NaOH (1 mol/L) and HCl (1 mol/L) solutions were used to change the pH of the three different ionic strengths of Na-Mt suspensions. The pH was increased or decreased incrementally by adding the base or an acid, so as not to cause excessive dilution to the samples. The prepared samples were then sonicated with an ultrasonic processor UH-250A (400 W and 20 kHz) and a sound enclosure UH-S2 (Jinghui Ltd., Shenzhen, China) for three times (at least 60 s at 80% amplitude for each time) and left to cool. Then, the samples were shaken overnight to make sure the suspensions at different pH were stabilized. The pH was measured with a PHSJ-3F pH electrode and a pH meter (INESA, Shanghai, China). Finally, the three different ionic strengths of samples were respectively adjusted to the endpoint of pH around 6.0, 7.7, 8.1, and 9.2, respectively.

2.2. Zeta Potential Measurements

Zeta potential measurements of Na-montmorillonite, Al₂O₃, and SiO₂ were carried out using a Nano-ZS zeta potential analyzer (Malvern, Worcestershire, UK). An average value of three measurements was taken to represent a reported zeta potential of Na-Mt suspension for a given condition. The Na-Mt samples for zeta potential measurements were using the adjusted salt-pH Na-Mt. The Al₂O₃ and SiO₂ samples (1 g) were dispersed in 200 mL of 10⁻² M NaCl solution by stirring at 500 rpm for about 30 min, separately. Then, each suspension was adjusted with variable pHs ranging between 3 and 9. After that, 1.5 mL suspension was transferred to a sample cell for zeta potential measurements. In this work, we used Al₂O₃ and SiO₂ to simulate the surface groups of montmorillonite edges. The zeta potential of montmorillonite edges (ζ_{edge}) can be calculated by Equation (1) [9,17]:

$$\zeta_{\text{edge}} = \frac{1}{3} (\zeta_{\text{SiO}_2} + 2\zeta_{\text{Al}_2\text{O}_3}) \quad (1)$$

where ζ_{SiO_2} and $\zeta_{\text{Al}_2\text{O}_3}$ are the zeta potential of Al₂O₃ and SiO₂, respectively.

2.3. Sedimentation and Transmittance Measurements

Prior to sedimentation and filtration experiments, the different types of prepared Na-montmorillonite suspensions ($C_c = 1$ g/L) were stirred using a stirrer at 350 rpm for 6 h to obtain a homogenous and representative sample. The constant and proper velocity of stirring allows the Na-Mt particles throughout the suspension and also avoids the particle structure to be broken by an excessive shear. After the stir was completed, 250 mL of each prepared sample was taken and then placed in a measuring cylinder with a stopper. The diameter of the 250 mL measuring cylinder was 42 mm. The height of the sediment bed and the test of transmittance were measured after the samples settled for 12 h. The liquids for transmittance tests were taken from the sediment bed, located at the 30 mL tick mark of the measuring cylinder, with an adjustable volume pipettor. The test was measured by a 721 visible spectrophotometer (Shanghai Jinghua Ltd., Shanghai, China) and the ultraviolet rays (UV) were set at 800 nm.

2.4. Rheological Measurements

The rheological measurements were performed with an NDJ-9S rotational viscometer (Shanghai Pingxuan Ltd., Shanghai, China) using a small sample of salt-pH Na-montmorillonite suspension (30 mL). The sample was stirred slowly with a magnetic stirrer for 5 min in a low constant temperature trough, which was set at 25 °C. This step was in case the sample settled and also prevented the particle structure from being broken by stirring. Then, the sample was introduced into a rotating outer cylinder carefully. After the rotating inner cylinder ($\varphi = 12.5$ mm) and the fixed outer cylinder ($\varphi = 15$ mm) were settled, viscometric data were obtained at a rotational speed of 60 rpm. Each value was recorded for 6 to 8 times and averaged at the end. The shear rate of the inner cylinder wall ($\dot{\gamma}_1$) was calculated from the following Equation (2):

$$\dot{\gamma}_1 = \frac{4\pi N}{60 \left[1 - \left(\frac{R_1}{R_2} \right)^2 \right]}, \quad (2)$$

where N is the rotational speed, R_1 is the radii of the rotating inner cylinder, and R_2 is the radii of the outer cylinder. According to the rotational speed, the shear rate was calculated to be 41.11 s⁻¹.

2.5. Filtration Measurements

A schematic of the experimental filtration devices is shown in Figure 4. The system includes a conditioning tank with an impeller for stirring, a filtration unit with a sand core, a 250 mL vacuum flask, an HD camera for recording data, and a vacuum pump with a vacuum and a pressure regulator.

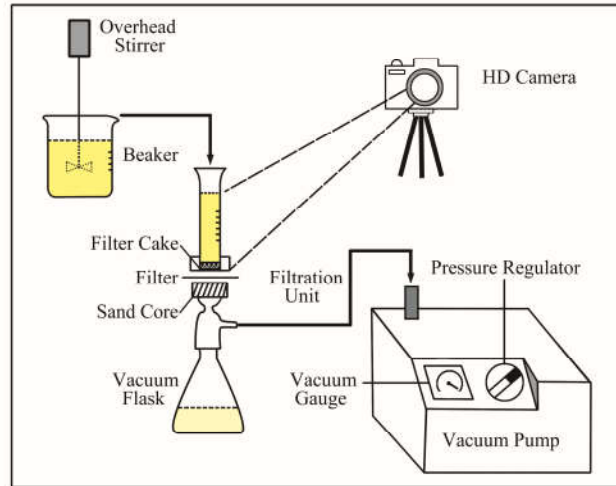


Figure 4. A schematic diagram of the experimental filtration devices.

The filtration experiments were carried out with different ionic strengths and pH of Na-montmorillonite samples at an indoor temperature of 25 ± 2 °C. The sample was placed into a 500 mL beaker and stirred at 350 rpm for 6 h. Then, 20 mL of the sample from the beaker was carefully transferred into the measuring cylinder without spillage. The 0.45 μm of millipore filter membrane was made by polypropylene and placed on the filtration unit with a sand core. The pressure valve was opened after the sample was transferred, and the pressure was adjusted to 0.06 MPa. The HD camera and a stopwatch were then initiated to record the volume of the sample and filtration time, in order to evaluate the filtration rate. The filtration experiment was finished when all 20 mL of the liquid sample had been filtrated.

The average specific cake resistance α_{av} for the constant pressure of filtration was calculated using experimental data and equations based on Darcy's law (Equation (3)). The procedure of determining α_{av} from experimental data is widely applied, and has been introduced in the literature [31,32]. The integrated form of the general filtration equation (Equation (3)) is given by:

$$\frac{t}{V} = \frac{\alpha_{av}\mu c}{2A^2\Delta P}V + \frac{\mu R_m}{A\Delta P}, \quad (3)$$

where t is filtration time (s), V is the volume of filtrate (m^3), α_{av} is the average specific cake resistance (m/kg), μ is the viscosity of the liquid ($\text{Pa}\cdot\text{s}$), c is the filtration concentration (kg/m^3), A is the filtration area (m^2), ΔP is the pressure difference (Pa), and R_m is the resistance of the filter medium (m^{-1}). In this work, the resistance of the cake [33]:

$$\alpha_{av} = \frac{2aA^2\Delta P}{\mu c}, \quad (4)$$

where a is the symbol for the experimentally determined slope t/V^2 in the calculation.

3. Results

3.1. Zeta Potential Experiments

Zeta potentials of Al_2O_3 , SiO_2 , and Na-montmorillonite edges at different pHs in the presence of 10^{-2} M NaCl are shown in Figure 5. As can be seen, the points of zero charge of the edge surface of Na-Mt ($\text{pH}_{\text{PZC,edge}}$) were sites at $\text{pH} = 6.8$, which is consistent with the reported value $\text{pH} \sim 6.5\text{--}7$ [9,15–17]. When the $\text{pH} < 6.8$, the zeta potential results of Na-Mt edges were positive. On the contrary, the Na-Mt edges were negatively charged at $\text{pH} > 6.8$. The zeta potentials of the total surface of Na-Mt were plotted with respect to increasing salt concentration as a function of pH as shown in Figure 6. With

the salt concentration increased from 10^{-3} to 10^{-1} M, the absolute value of zeta potential was decreased. The changes of pH also showed significant difference on the surface charge of Na-Mt. In NaCl concentrations of 10^{-3} and 10^{-2} M, the trends of zeta potential both showed a sharp decline with an increasing pH. Compared with the results in low NaCl concentration, the zeta potential of the Na-Mt surface was slightly reduced from -23.6 to -28.8 mV with pH increased from 6.0 to 9.2 in NaCl concentration of 10^{-1} M.

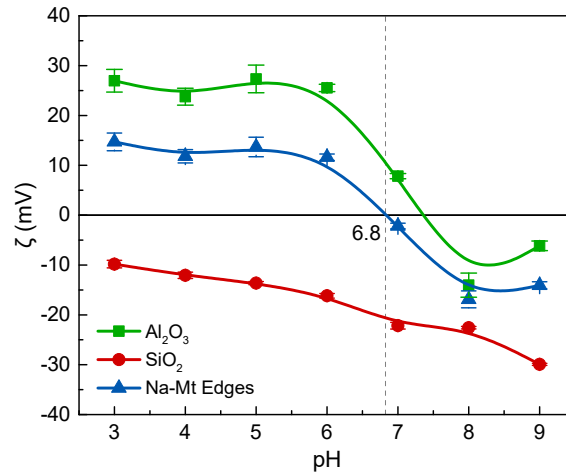


Figure 5. The changes in zeta potential of Al₂O₃, SiO₂, and Na-Mt edges as a function of pH in the presence of 10^{-2} M NaCl concentration.

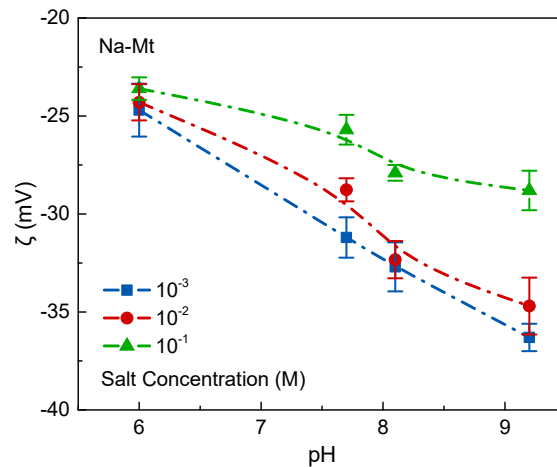


Figure 6. The changes in zeta potential of Na-Mt surface with respect to increasing salt concentration as a function of pH.

3.2. Sedimentation and Transmittance Experiments.

The sediment being settled for 12 h, the height of the sediment bed and transmittance at different pHs as a function of salt concentration are presented in Figures 7,8. It should be noticed that the sedimentation results of pH ~ 6.0 were quite different from those under basic conditions (pH $>$ pHPZC,edge). With low salt concentration (10^{-3} M), the montmorillonite particles were coagulated at pH ~ 6 , and the sediment height and transmittance of it were 192 mL and 52.4%, respectively. However, under basic conditions, the particles were dispersed and stabilized in the suspension, without the obvious interface between supernatant and sediment bed. With the addition of salt concentration to

10^{-2} M, the sedimentation velocity was accelerated, and both the height of the sediment bed and transmittance were much lower at $\text{pH} \sim 6$. Meanwhile, under basic conditions, the sediment height showed a slight reduction of about 5–15 mL, and the boundary between supernatant and sediment bed was clear. When the salt concentration reached 10^{-1} M, except the height at $\text{pH} \sim 6$, the other plots show that particles were coagulated rapidly in the basic suspension because of the height of the sediment bed and transmittance was decreased sharply. With pH increased from 7.7 to 9.2, the sediment bed was decreased from 156 mL to 78 mL, and transmittance was decreased from 51.8% to 20.7%. Overall, adding NaCl promoted the coagulation of particles and sedimentation velocity of suspensions at all pH values, and reduced the height of the sediment bed and transmittance. In particular, at the high salt concentration (10^{-1} M), the suspensions all settled rapidly. Additionally, compared with the sedimentation results at $\text{pH} > \text{pH}_{\text{PZC,edge}}$, the results at $\text{pH} \sim 6$ in Figure 7a show a quite different tendency.

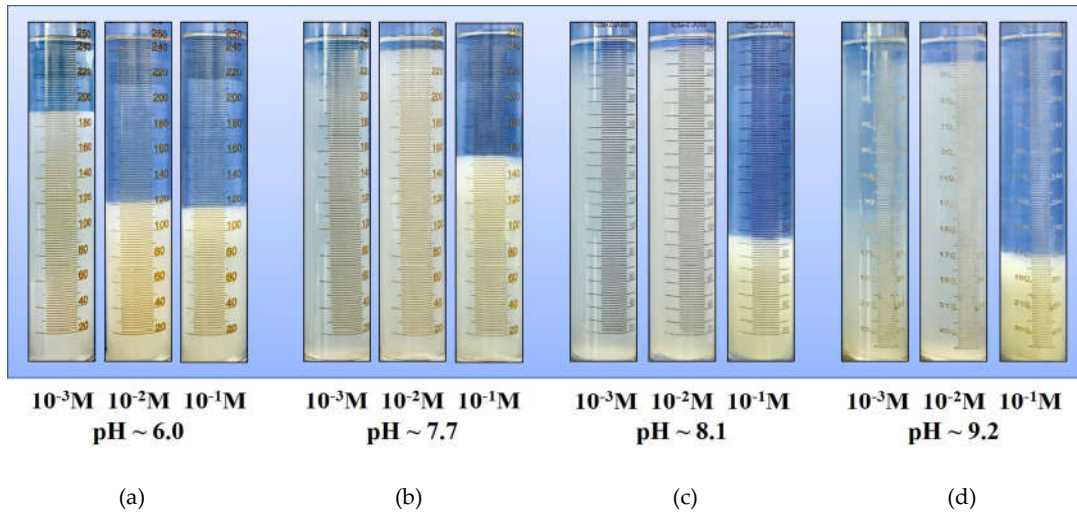


Figure 7. Photos of the Na-Mt suspensions taken after settling for 12 h under different NaCl concentration (10^{-3} , 10^{-2} , 10^{-1} M) and pH : (a) $\text{pH} \sim 6.0$; (b) $\text{pH} \sim 7.7$; (c) $\text{pH} \sim 8.1$; (d) $\text{pH} \sim 9.2$.

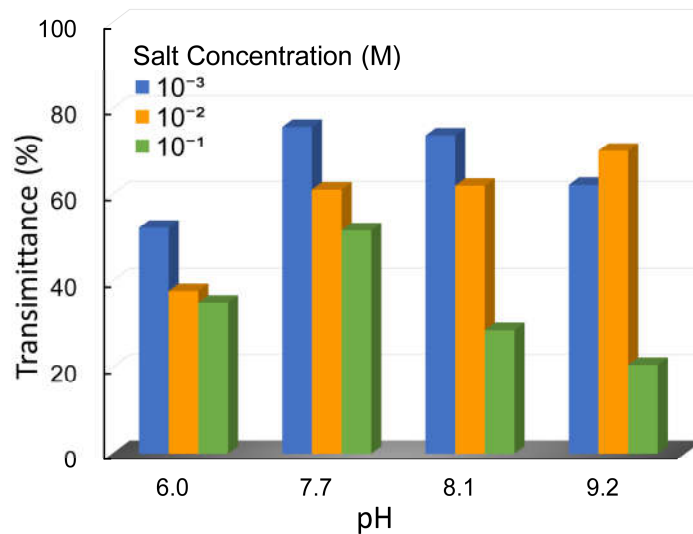


Figure 8. The changes in transmittance of Na-Mt suspensions through the sedimentation process with respect to increasing salt concentration as a function of pH . The test samples were taken from the 30 mL tick mark of the measuring cylinder.

3.3. Rheology Experiments

For the rheological property, the apparent viscosity of suspensions as a function of salt concentration in a pH range from 6.0 to 9.2 is plotted in Figure 9. The apparent viscosity was measured with a constant shear rate: 41.11 s^{-1} . In this figure, there was still an obvious difference between $\text{pH} \sim 6$ ($\text{pH} < \text{pH}_{\text{PZC,edge}}$) and the basic conditions ($\text{pH} > \text{pH}_{\text{PZC,edge}}$). The minimums of apparent viscosity appeared in low salt concentration (10^{-3} M) at $\text{pH} 7.7, 8.1,$ and 9.2 , and the apparent viscosity for those cases were $0.95, 0.98,$ and $1.02 \text{ mPa}\cdot\text{s}$, respectively. The apparent viscosity of $\text{pH} \sim 6$ was much higher than that of basic suspensions in salt concentrations of 10^{-3} and 10^{-2} M , which were 1.31 and $1.64 \text{ mPa}\cdot\text{s}$, respectively. However, when salt concentration increased to 10^{-1} M , the apparent viscosity was increased to the maximums at $\text{pH} 7.7, 8.1,$ and 9.2 , which were $1.81, 1.87,$ and $1.63 \text{ mPa}\cdot\text{s}$, respectively. At $\text{pH} \sim 6$, the apparent viscosity was increased with the increase in salt concentration from 10^{-3} to 10^{-2} M , and then with an exponential increase in salt concentration to 10^{-1} M , the apparent viscosity had no significant effect. At $\text{pH} > \text{pH}_{\text{PZC,edge}}$, the plots show a similar tendency: the apparent viscosity increased slightly at 10^{-2} M NaCl and sharply at 10^{-1} M NaCl.

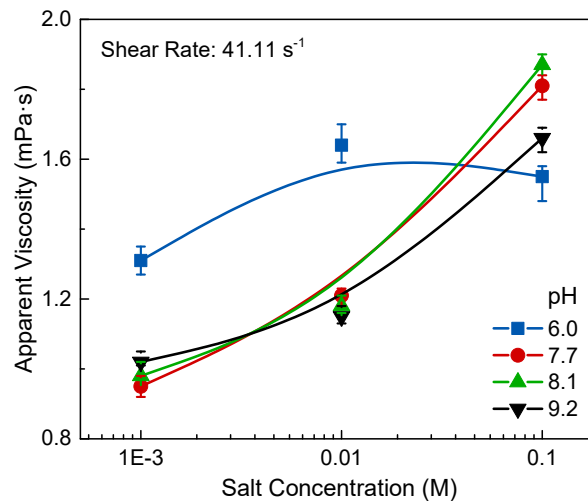


Figure 9. The changes in apparent viscosity of suspensions with respect to different pH as a function of salt concentration.

3.4. Filtration Experiments

Figure 10 presents the plots for filtration performance at different pHs and salt concentrations, which were described by Darcy's law (Equation (3)). The calculation of the average specific resistance of filter cake (α) can be conducted using the gradient. Such gradients, remarkably, can be calculated from filtration time/filtration volume, a dependent variable, and filtrate volume, an independent variable. The corresponding data are plotted in Figure 11. As indicated in these figures, whether increasing salt concentration or pH, filtration performance was promoted, and filtration time and α were decreased, apparently. On the one hand, the filtration rate increased as a function of pH with constant salt concentration. As depicted in Figure 10a, it can be observed that an increase of pH from 6.18 to 9.14 resulted in the filtration time for the same 20 mL volume of suspensions being reduced by over fivefold from around 370 to just 65 min in low salt concentration (10^{-3} M). This tendency can also be observed in Figure 10b,c. On the other hand, the time to finish a filtration run was reduced significantly with the addition of salt concentration. At pH around 8.1, the filtration time in salt concentrations of $10^{-3}, 10^{-2},$ and 10^{-1} M was 99, 32, and 2 min, respectively. This tendency of accelerating the filtration rate with salt concentration was also found at other pHs. Moreover, a markedly different result between both sides of $\text{pH}_{\text{PZC,edge}}$ appeared in high salt concentration as shown in Figure 10c.

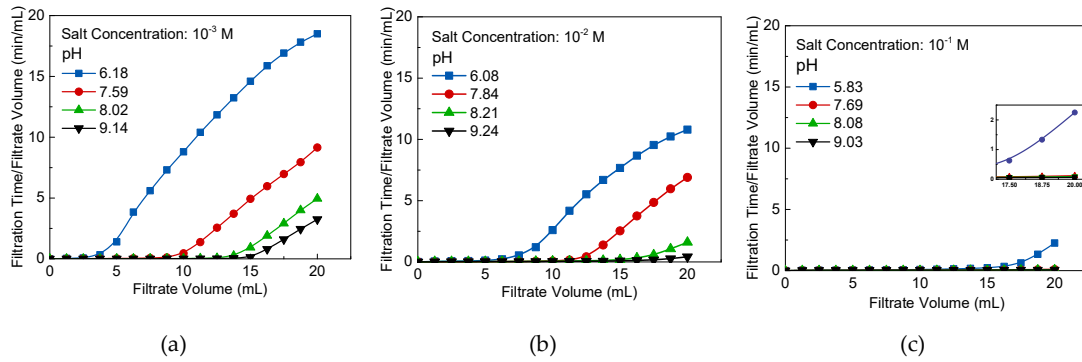


Figure 10. Darcy plot for the filtration of Na-Mt suspensions with respect to different pHs as a function of salt concentration: (a) 10^{-3} M; (b) 10^{-2} M; (c) 10^{-1} M.

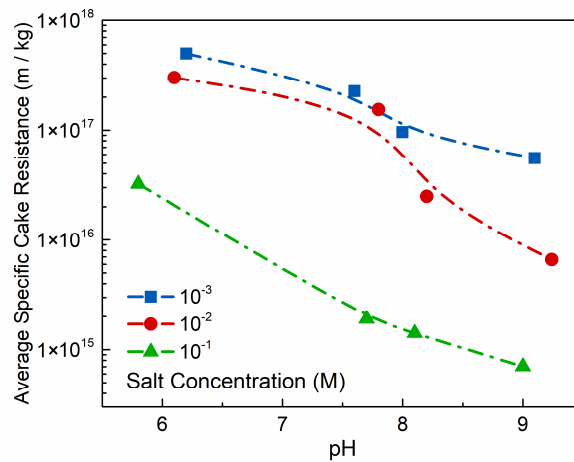


Figure 11. The changes in average specific cake resistance through the filtration process with respect to increasing salt concentration as a function of pH.

4. Discussion

The dispersed and coagulated states of montmorillonite particles are closely related to the surface charges, which in turn are a function of the electrolyte concentration and pH. As mentioned in the introduction, the main contributions to the surface charges of montmorillonite are the permanent negative charges on the basal plane by the isomorphous substitution and pH-dependent charges on the edge [34]. The results of zeta potential experiments were also consistent with this theory as shown in Figure 5 and Figure 6. In this work, the point of zero charge of edge surface ($\text{pH}_{\text{PZC,edge}}$) was the site at $\text{pH} = 6.8$. When $\text{pH} \sim 6.0 < \text{pH}_{\text{PZC,edge}}$, the Na-montmorillonite layers with edge^+ and face^- are anisotropically coagulated by electrostatic attraction (Figure 10b). Since the acidic Na-Mt suspensions are very sensitive to salts, particles coagulate spontaneously at a very low salt concentration, as shown in Figure 7a. When the pH is increased beyond the point of zero charge of the edges, the edges become negatively charged. Due to the effect of electrostatic repulsion, the Na-Mt particles dispersed with a stable distance in the dilute suspensions at the salt concentration of 10^{-3} M (Figure 10a). The dispersed suspensions presented without a sharp interface between supernatant and sediment bed in sedimentation experiments as shown in Figure 7, and also had the minimum apparent viscosity in rheology experiments as shown in Figure 9. However, as the electrolyte concentration increased, the NaCl increased the concentration of the counterions in the particle diffusion layer and some counterions were squeezed out of the stern layer. Thereby, the potential of the electric double layer decreased, causing the diffusion layer to be compressed and the electrostatic repulsion between the particles to decrease. With the increase of NaCl concentration at $\text{pH} >$

$pH_{pZC,edge}$, Na-Mt suspension prefers to form as isotropic samples, and continuing to increase the addition of NaCl, the Van der Waals attraction as a short-range applied force increases significantly and overcomes the electrostatic repulsion until the distance between particles reduces to a certain extent. The Na-Mt particles coagulate as Face/Face network structure ultimately (Figure 12c). The sedimentation results in NaCl concentration from 10^{-2} to 10^{-1} M at $pH > pH_{pZC,edge}$ is consistent with this theory. Gabriel, J. et al. [35] previously used polarized light microscopy to observe the textures of birefringent gels and also found these coagulation behaviors of isotropic and stabilized nematic phase at NaCl concentrations ranging from 10^{-2} to 10^{-1} M. The size of coagulated flocs enlarged with the increase of salt concentration [15]. The sedimentation rate accelerated and the sediment bed reduced with an increase in salt concentration, which is shown in Figure 7. The rheological behavior of a suspension can sensitively indicate the interactions between particles [2,36]. The rheology of Na-Mt suspension is affected by its dispersion, arrangement, and association mode between particles. As observed in Figure 9, the behavior of Na-Mt suspension is influenced by the gradually formed band-type network structure (Face/Face), which can prominently improve the apparent viscosity with the increase of salt concentration.

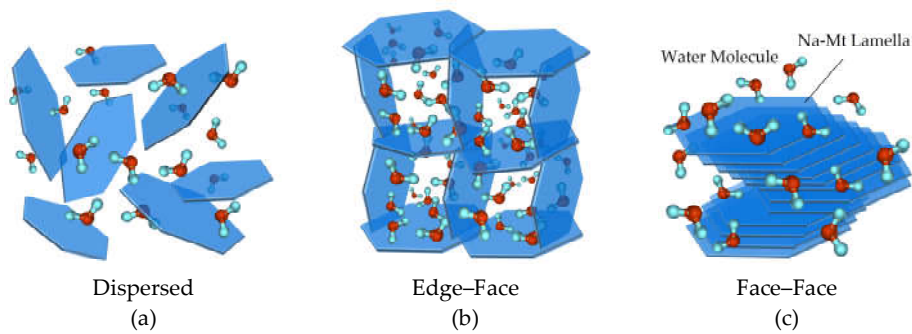


Figure 12. Schematic diagrams of the dispersed and aggregated modes of Na-Mt particles in suspensions and distribution of water molecules: (a) dispersed state; (b) aggregated Edge-Face mode; (c) aggregated Face-Face mode.

However, the coagulation and rapid settling of mineral particles in the suspension does not necessarily represent the optimal conditions for the dewatering process, as observed in Figures 7 and 11. Rheological properties affect the stability of the network structure of filter cake, and further affect the porosity of cake and the permeability of water [37,38]. The influence of electrolyte concentration and pH on the interaction between particles, as well as the different coagulation modes, plays an important role in the vacuum filtration process. We found that the filtration efficiency of the anisotropic three-dimensional card-house network structure flocs (Edge/Face association) is much lower than the Face/Face coagulation at a similar sedimentation rate and height of sediment bed, which is even lower than the dispersed state of suspension in the same NaCl concentration. Santiwong, S.R et al. [39] found that the opposite effect is related to a change in arrangements of particles or particle assemblages in filter cakes, although the Face/Face mode coagulation formed a more compact and less permeable filter cake. Benna, M. [40] also observed that the filter cake is the thickest and contains the most moisture ratio at acidic pH. Therefore, we conjecture that the anisotropic three-dimensional card-house network structure has a relatively sealed structure space in the aqueous solution. With this special structure, it is difficult for water molecules to flow out of the structure space under the action of external forces. Besides, it affects the removal of water molecules in the filtration process seriously [41–43], as shown in Figure 12b. In Figure 11, the average specific cake resistance as an important parameter to measure the ease of filtration is decreased with pH and salt concentration increase. In terms of the impact on pH, increasing pH leads to the edge-OH⁻ transformation into edge-OH₂⁻ due to the increasing OH⁻ in the suspension [15]. Due to the Edge/Face connection breaking gradually, water molecules become free water, which is beneficial to the dewatering process. Tombacz, E. and Szekecs, M. [15] also found that the formation of layers

ordered in parallel to each other with pH increased, because the intensity of basal plane reflection increased markedly with increasing pH. In terms of impact on salt concentration, Edge/Face interaction reduces with the increasing salt concentration at $\text{pH} < \text{pH}_{\text{PZC,edge}}$. However, the addition of electrolyte also suppresses the electrical double layer on the particle surfaces and the shielding effect of the extended double layers at the edges is reduced [44]. Thus, addition of salt concentration will not induce the Face/Face network structure, and Edge/Face mode coagulation will still form with reduction of floc strength. This will facilitate the removal of water molecules in the network structure under external forces. At $\text{pH} > \text{pH}_{\text{PZC,edge}}$, the effect of salt concentration on the electric double layer will inhibit the osmotic expansion and reduce the water molecules between the Na-Mt layers [45,46]. At high salt concentration, the Na-Mt layers coagulated by overlapping of the faces, forming large flocs with Face/Face network structure, as shown in Figure 12c. In this case, the water molecules in the structure space are reduced greatly, and they are easier to be squeezed out.

5. Conclusions

The Na-Mt suspension is adjusted by pH and salt concentration so that the surface charge of the Na-Mt particles changes. The positive or negative charge of the pH-dependent edge is formed by the transfer of H^+ or OH^- from the aqueous phase. Increasing the salt concentration can inhibit the development of the electric double layer of the particles. Two factors change the interaction force between particles, making them appear in dispersed or coagulated state in the suspension, which is reflected in sedimentation, rheology, and filtration experiments. When $\text{pH} < \text{pH}_{\text{PZC,edge}}$, the Na-Mt suspension can coagulate spontaneously at low salt concentration. However, when pH increases over $\text{pH}_{\text{PZC,edge}}$, the coagulation does not occur until the salt concentration increases to 10^{-1} M. Besides, with the increases of pH or salt concentration, the viscosity and filtration rate increase, and the average specific cake resistance reduces. We propose that this phenomenon is related to the change of particle coagulation structure in the suspension, but further work should be conducted to verify this. In other words, coagulation or rapid settling is not the necessary condition to enhance filtration performance. Specifically, the three-dimensional Edge/Face network structure in Na-Mt suspension is relatively sealed and may block water molecules from being squeezed out of the structure in the filtration process. However, with the increasing of pH value and electrolyte concentration, the overlapping Face/Face association reduces the interlayer spacing and interlayer water molecules, thus enhancing the filtration performance significantly.

Author Contributions: Conceptualization, H.L. and X.D.; data curation, Y.D.; formal analysis, Y.D.; funding acquisition, H.L. and X.D.; investigation, Y.D.; methodology, H.L. and Y.F.; project administration, Y.F. and D.S.; resources, X.D.; supervision, Z.G. and X.D.; validation, X.M. and Y.W.; visualization, Y.D.; writing—original draft preparation, Y.D.; writing—review and editing, Y.D., Y.W., and Z.G. All authors have read and agreed to the published version of the manuscript.

Funding: This research was funded by International (Regional) Cooperation and Exchange Projects of the National Natural Science Foundation of China (No. 51820105006), National Natural Science Foundation of China (No. 51674174), and Natural Science Youth Foundation of China (No. 51804213).

Conflicts of Interest: The authors declare no conflict of interest.

References

1. Lagaly, G.; Ziesmer, S. Colloid chemistry of clay minerals: The coagulation of montmorillonite dispersions. *Adv. Colloid Interface Sci.* **2003**, *100*, 105–128, doi:10.1016/S0001-8686(02)00064-7.
2. Choo, K.Y.; Bai, K. Effects of bentonite concentration and solution pH on the rheological properties and long-term stabilities of bentonite suspensions. *Appl. Clay Sci.* **2015**, *108*, 182–190, doi:10.1016/j.clay.2015.02.023.
3. Abu-Jdayil, B. Rheology of sodium and calcium bentonite–water dispersions: Effect of electrolytes and aging time. *Int. J. Miner. Process.* **2011**, *98*, 208–213, doi:10.1016/j.minpro.2011.01.001.
4. Li, W.; Wang, J.; Xu, D. Molecular simulations of the effect of hydrated montmorillonite on the viscosity of polyacrylamide under confined shear. *J. Wuhan Univ. Technol. Mater. Sci. Ed.* **2015**, *30*, 556–561, doi:10.1007/s11595-015-1188-4.

5. Goh, R.; Leong, Y.-K.; Lehane, B. Bentonite slurries—Zeta potential, yield stress, adsorbed additive and time-dependent behaviour. *Rheol. Acta* **2010**, *50*, 29–38, doi:10.1007/s00397-010-0498-x.
6. Rand, B.; Pekenć, E.; Goodwin, J.W.; Smith, R.W. Investigation into the existence of edge—Face coagulated structures in Na-montmorillonite suspensions. *J. Chem. Soc. Faraday Trans. 1 Phys. Chem. Condens. Phases* **1980**, *76*, 225–235, doi:10.1039/F19807600225.
7. Adachi, Y.; Di, C.; Xiao, F.; Kobayashi, M. Size, orientation, and strength of Na-montmorillonite flocs flowing in a laminar shear flow. *Colloid Polym. Sci.* **2019**, *297*, 979–987, doi:10.1007/s00396-019-04532-3.
8. Lagaly, G. Principles of flow of kaolin and bentonite dispersions. *Appl. Clay Sci.* **1989**, *4*, 105–123, doi:10.1016/0169-1317(89)90003-3.
9. Duran, J.D.; Ramos-Tejada, M.M.; Arroyo, F.J.; Gonzalez-Caballero, F. Rheological and Electrokinetic Properties of Sodium Montmorillonite Suspensions. *J. Colloid Interface Sci.* **2000**, *229*, 107–117, doi:10.1006/jcis.2000.6956.
10. Huang, W.A.; Leong, Y.K.; Chen, T.; Au, P.I.; Liu, X.H.; Qiu, Z.S. Surface chemistry and rheological properties of API bentonite drilling fluid: pH effect, yield stress, zeta potential and ageing behaviour. *J. Pet. Sci. Eng.* **2016**, *146*, 561–569, doi:10.1016/j.petrol.2016.07.016.
11. Au, P.I.; Leong, Y.K. Rheological and zeta potential behaviour of kaolin and bentonite composite slurries. *Colloids Surf. A Physicochem. Eng. Asp.* **2013**, *436*, 530–541, doi:10.1016/j.colsurfa.2013.06.039.
12. Baik, M.H.; Lee, S.Y. Colloidal stability of bentonite clay considering surface charge properties as a function of pH and ionic strength. *J. Ind. Eng. Chem.* **2010**, *16*, 837–841, doi:10.1016/j.jiec.2010.05.002.
13. Janek, M.; Lagaly, G. Proton saturation and rheological properties of smectite dispersions. *Appl. Clay Sci.* **2001**, *19*, 121–130, doi:10.1016/S0169-1317(01)00051-5.
14. Penner, D.; Lagaly, G. Influence of anions on the rheological properties of clay mineral dispersions. *Appl. Clay Sci.* **2001**, *19*, 131–142, doi:10.1016/S0169-1317(01)00052-7.
15. Tombácz, E.; Szekeres, M. Colloidal behavior of aqueous montmorillonite suspensions: The specific role of pH in the presence of indifferent electrolytes. *Appl. Clay Sci.* **2004**, *27*, 75–94, doi:10.1016/j.clay.2004.01.001.
16. Chang, F.-R.C.; Sposito, G. The Electrical Double Layer of a Disk-Shaped Clay Mineral Particle: Effect of Particle Size. *J. Colloid Interface Sci.* **1994**, *163*, 19–27, doi:10.1006/jcis.1994.1076.
17. Sondi, I.; Milat, O.; Pravdić, V. Electrokinetic Potentials of Clay Surfaces Modified by Polymers. *J. Colloid Interface Sci.* **1997**, *189*, 66–73, doi:10.1006/jcis.1996.4753.
18. Morris, G.E.; Zbik, M.S. Smectite suspension structural behaviour. *Int. J. Miner. Process.* **2009**, *93*, 20–25, doi:10.1016/j.minpro.2009.05.003.
19. Karnland, O.; Olsson, S.; Nilsson, U. *Mineralogy and Sealing Properties of Various Bentonites and Smectite-Rich Clay Materials*; Swedish Nuclear Fuel and Waste Management Co.: Stockholm, Sweden, 2006.
20. Segad, M.; Jonsson, B.; Akesson, T.; Cabane, B. Ca/Na montmorillonite: Structure, forces and swelling properties. *Langmuir* **2010**, *26*, 5782–5790, doi:10.1021/la9036293.
21. Duc, M.; Gaboriaud, F.; Thomas, F. Sensitivity of the acid-base properties of clays to the methods of preparation and measurement. 2. Evidence from continuous potentiometric titrations. *J. Colloid Interface Sci.* **2005**, *289*, 148–156, doi:10.1016/j.jcis.2005.03.057.
22. Michot, L.J.; Bihannic, I.; Thomas, F.; Lartiges, B.S.; Waldvogel, Y.; Caillet, C.; Thieme, J.; Funari, S.S.; Levitz, P. Coagulation of Na-montmorillonite by inorganic cations at neutral pH. A combined transmission X-ray microscopy, small angle and wide angle X-ray scattering study. *Langmuir* **2013**, *29*, 3500–3510, doi:10.1021/la400245n.
23. Doi, A.; Ejtemaei, M.; Nguyen, A.V. Effects of ion specificity on the surface electrical properties of kaolinite and montmorillonite. *Miner. Eng.* **2019**, *143*, 105929, doi:10.1016/j.mineng.2019.105929.
24. Wu, M.Y.; Adachi, Y. Effects of electrolyte concentration and pH on the sedimentation rate of coagulated suspension of sodium montmorillonite. *Colloids Surf. A Physicochem. Eng. Asp.* **2016**, *506*, 686–693, doi:10.1016/j.colsurfa.2016.07.027.
25. Wu, M.-Y.; Adachi, Y. Duration of initial flocculation stage in the sedimentation of sodium montmorillonite suspension in the semi-dilute regime. *Colloid Polym. Sci.* **2017**, *296*, 71–76, doi:10.1007/s00396-017-4222-6.
26. Benna, M.; Kbir-Arighuib, N.; Clinard, C.; Bergaya, F. Static filtration of purified sodium bentonite clay suspensions. Effect of clay content. *Appl. Clay Sci.* **2001**, *19*, 103–120, doi:10.1016/S0169-1317(01)00050-3.
27. Barry, M.M.; Jung, Y.; Lee, J.-K.; Phuoc, T.X.; Chyu, M.K. Fluid filtration and rheological properties of nanoparticle additive and intercalated clay hybrid bentonite drilling fluids. *J. Pet. Sci. Eng.* **2015**, *127*, 338–346, doi:10.1016/j.petrol.2015.01.012.

28. Luo, Z.; Pei, J.; Wang, L.; Yu, P.; Chen, Z. Influence of an ionic liquid on rheological and filtration properties of water-based drilling fluids at high temperatures. *Appl. Clay Sci.* **2017**, *136*, 96–102, doi:10.1016/j.clay.2016.11.015.
29. Yang, L.; Jiang, G.; Shi, Y.; Lin, X.; Yang, X. Application of ionic liquid to a high-performance calcium-resistant additive for filtration control of bentonite/water-based drilling fluids. *J. Mater. Sci.* **2017**, *52*, 6362–6375, doi:10.1007/s10853-017-0870-7.
30. Benna, M.; Kbir-Arighuib, N.; Magnin, A.; Bergaya, F. Effect of pH on Rheological Properties of Purified Sodium Bentonite Suspensions. *J. Colloid Interface Sci.* **1999**, *218*, 442–455, doi:10.1006/jcis.1999.6420.
31. Alam, N.; Ozdemir, O.; Hampton, M.A.; Nguyen, A.V. Dewatering of coal plant tailings: Flocculation followed by filtration. *Fuel* **2011**, *90*, 26–35, doi:10.1016/j.fuel.2010.08.006.
32. Kinnarinen, T.; Tuunila, R.; Hakkinen, A. Reduction of the width of particle size distribution to improve pressure filtration properties of slurries. *Miner. Eng.* **2017**, *102*, 68–74, doi:10.1016/j.mineng.2016.12.009.
33. Huttunen, M.; Nygren, L.; Kinnarinen, T.; Hakkinen, A.; Lindh, T.; Ahola, J.; Karvonen, V. Specific energy consumption of cake dewatering with vacuum filters. *Miner. Eng.* **2017**, *100*, 144–154, doi:10.1016/j.mineng.2016.10.025.
34. Olphen, H.V. *An Introduction to Clay Colloid Chemistry, for Clay Technologists, Geologists, and Soil Scientists*; Wiley Interscience: New York, NY, USA, 1977.
35. Gabriel, J.-C.P.; Sanchez, C.; Davidson, P. Observation of Nematic Liquid-Crystal Textures in Aqueous Gels of Smectite Clays. *J. Phys. Chem.* **1996**, *100*, 11139–11143, doi:10.1021/jp961088z.
36. Czibulya, Z.; Tombácz, E.; Szegi, T.; Michéli, E.; Zsolnay, Á. Standard state of soil dispersions for rheological measurements. *Appl. Clay Sci.* **2010**, *48*, 594–601, doi:10.1016/j.clay.2010.03.009.
37. Chen, B.H.; Lee, S.J.; Lee, D.J. Rheological characteristics of the cationic polyelectrolyte flocculated wastewater sludge. *Water Res.* **2005**, *39*, 4429–4435, doi:10.1016/j.watres.2005.08.035.
38. Marinetti, M.; Dentel, S.K.; Malpei, F.; Bonomo, L. Assessment of rheological methods for a correlation to sludge filterability. *Water Res.* **2010**, *44*, 5398–5406, doi:10.1016/j.watres.2010.06.046.
39. Santiwong, S.R.; Guan, J.; Waite, T.D. Effect of ionic strength and pH on hydraulic properties and structure of accumulating solid assemblages during microfiltration of montmorillonite suspensions. *J. Colloid Interface Sci.* **2008**, *317*, 214–227, doi:10.1016/j.jcis.2007.09.052.
40. Benna, M.; Kbir-Arighuib, N.; Clinard, C.; Bergaya, F. Card-house microstructure of purified sodium montmorillonite gels evidenced by filtration properties at different pH. In *Adsorption and Nanostructure*; Springer: Berlin/Heidelberg, Germany, 2002; pp. 204–210.
41. Bergaya, F.; Lagaly, G. General Introduction. In *Handbook of Clay Science*; Elsevier: Amsterdam, The Netherlands, 2013; pp. 1–19, doi:10.1016/b978-0-08-098258-8.00001-8.
42. Du, J.; Morris, G.; Pushkarova, R.A.; St. C. Smart, R. Effect of Surface Structure of Kaolinite on Aggregation, Settling Rate, and Bed Density. *Langmuir* **2010**, *26*, 13227–13235, doi:10.1021/la100088n.
43. Zhao, Y.; Yi, H.; Jia, F.; Li, H.; Peng, C.; Song, S. A novel method for determining the thickness of hydration shells on nanosheets: A case of montmorillonite in water. *Powder Technol.* **2017**, *306*, 74–79, doi:10.1016/j.powtec.2016.10.045.
44. Heath, D.; Tadros, T.F. Influence of pH, electrolyte, and poly(vinyl alcohol) addition on the rheological characteristics of aqueous dispersions of sodium montmorillonite. *J. Colloid Interface Sci.* **1983**, *93*, 307–319, doi:10.1016/0021-9797(83)90415-0.
45. Rao, S.M.; Thyagaraj, T.; Raghuvier Rao, P. Crystalline and Osmotic Swelling of an Expansive Clay Inundated with Sodium Chloride Solutions. *Geotech. Geol. Eng.* **2013**, *31*, 1399–1404, doi:10.1007/s10706-013-9629-3.
46. Zhang, J.-F.; Zhang, Q.-H.; Maa, J.P.Y. Coagulation processes of kaolinite and montmorillonite in calm, saline water. *Estuar. Coast. Shelf Sci.* **2018**, *202*, 18–29, doi:10.1016/j.ecss.2017.12.002.

